Title - The Wnt effector TCF7l2 promotes oligodendroglial differentiation by repressing autocrine BMP4-mediated signaling

Running Title – Autocrine control of BMP4 signaling by TCF7l2

Authors: Sheng Zhang[1,2,*], Yan Wang[1,2,*], Xiaoqing Zhu[1,2], Lanying Song[1,2], Edric Ma[1,2], Jennifer McDonough[3], Hui Fu[4], Franca Cambi[5], Judith Grinspan[6], and Fuzheng Guo[1,2,#]

Author affiliations:
1, Department of Neurology, School of Medicine, University of California, Davis, CA
2, Institute for Pediatric Regenerative Medicine (IPRM), Shriners Hospitals for Children / UC Davis School of Medicine, Sacramento, CA
3, Department of Biological Sciences, Kent State University, Kent, OH
4, Division of Life Sciences and Medicine, School of Basic Medical Sciences, University of Science and Technology of China, Anhui, China
5, Department of Neurology, Pittsburgh University, Pittsburgh, PA
6, Department of Neurology, The Children's Hospital of Philadelphia, Philadelphia, PA
*, co-first authors
#, corresponding author: Fuzheng Guo, Shriners Hospitals for Children / School of Medicine, UC Davis, c/o 2425 Stockton Blvd, Sacramento, CA. Email: fzguo@ucdavis.edu
ORCID: 0000-0003-3410-8389

Keywords: Type2 diabetes risk gene, Wnt effector; TCF7l2/TCF4; canonical Wnt/β-catenin; oligodendrocyte differentiation; myelination; canonical BMP4 signaling; BMP/SMAD signaling; repression

Acknowledgments:
We thank Dr. Andreas Hecht (University of Freiburg, Germany) for providing TCF7l2-E2, M1, and S2 expression vectors and Dr. Gino Cortopassi (UC Davis) for providing U87 cells. This study was funded by NIH/NINDS (R21NS109790 and R01NS094559) and by Shriners Hospitals for Children (85107-NCA-19, 84553-NCA-18, and 84307-NCAL).

Competing interests: none

Abstract:

Promoting oligodendrocyte differentiation represents a promising option for remyelination therapy for treating the demyelinating disease multiple sclerosis (MS). The Wnt effector TCF7l2 was upregulated in MS lesions and had been proposed to inhibit oligodendrocyte differentiation. Recent data suggest the opposite yet underlying mechanisms remain elusive. Here we unravel a previously unappreciated function of TCF7l2 in controlling autocrine bone morphogenetic protein (BMP4)-mediated signaling. Disrupting TCF7l2 results in oligodendroglial-specific BMP4 upregulation and canonical BMP4 signaling activation *in vivo*. Mechanistically, TCF7l2 binds to *Bmp4* gene regulatory element and directly represses its transcriptional activity. Functionally, enforced TCF7l2 expression promotes oligodendrocyte differentiation by reducing autocrine BMP4 secretion and dampening BMP4 signaling. Importantly, compound genetic disruption demonstrates that oligodendroglial-specific BMP4 deletion rescues arrested oligodendrocyte differentiation elicited by TCF7l2 disruption *in vivo*. Collectively, our study reveals a novel connection between TCF7l2 and BMP4 in oligodendroglial lineage and provides new insights into augmenting TCF7l2 for promoting remyelination in demyelinating disorders such as MS.

Introduction:

Blocked differentiation of myelin-forming oligodendrocytes (OLs) from oligodendrocyte progenitor cells (OPCs) is a major cause for remyelination failure in multiple sclerosis, the most common demyelinating disorder (Franklin and Gallo, 2014). Promoting OL differentiation represents a promising option for remyelination therapy in combination with current immunomodulatory therapy for treating MS (Harlow et al., 2015). Identifying upregulated molecular targets in MS will provide new insights into designing remyelination therapeutic options. The upregulation of the Wnt effector transcription factor 7-like 2 (TCF7l2) in MS brain lesions (Fancy et al., 2009) suggest that it might be a potential target for overcoming OL differentiation blockade.

TCF7l2 is one of the four members (TCF1, TCF7l1, TCF7l2, and LEF1) of the TCF/LEF1 family that transcriptionally activates the canonical Wnt/β-catenin signaling (Cadigan, 2012). Based on the inhibitory role of Wnt/β-catenin genetic activation in OL differentiation (Guo et al., 2015), TCF7l2 had been previously proposed as a negative regulator of OL differentiation by transcriptionally activating Wnt/β-catenin signaling (Fancy et al., 2009; He et al., 2007). However, subsequent genetic studies have convincingly demonstrated that TCF7l2 is a positive

regulator of OL differentiation that TCF7l2 play a minor role in activating Wnt/β-catenin in oligodendroglial lineage cells (Hammond et al., 2015; Zhao et al., 2016). In this context, the molecular mechanisms underlying TCF7l2-regulated OL differentiation remains incompletely understood. We previously reported that genetically disrupting TCF7l2 inhibited OL differentiation with concomitant upregulation of the canonical BMP4 signaling in the CNS (Hammond et al., 2015), suggesting that the Wnt effector TCF7l2 may promote OL differentiation by tightly controlling BMP4 signaling, an inhibitory pathway of OL development (Grinspan, 2020). In this study, we presented strong evidence unraveling a new mechanism of TCF7l2 in promoting OL differentiation by repressing autocrine BMP4 signaling.

Materials and Methods:

Animals: The transgenic mice used in our study were: Olig2-CreER^{T2} (Takebayashi et al., 2002), Plp-CreER^{T2} (RRID: IMSR_JAX:005975), Pdgfrα-*CreER^{T2}* (RRID: IMSR_ JAX:018280), Tcf7l2-floxed (RRID: IMSR_JAX:031436), Bmp4-floxed (RRID: IMSR_JAX: 016878). Cre transgene was always maintained as heterozygosity. All our animals were from C57BL/6 background and maintained in 12 h light/dark cycle with water and food. Our animal protocols were approved by the Institutional Animal Care and Use Committee at the University of California, Davis.

Gene conditional KO by tamoxifen treatment: Tamoxifen (T5648, sigma) was dissolved in a mixture of ethanol and sunflower seed oil (1:9, v/v) at 30 mg/ml. All our animals including non-Cre Control and cko were intraperitoneally administered at a dose of 200 µg/g body weight.

Magnetic-activated cell sorting (MACS): The forebrain was dissociated by the papain dissociation kit (LK003176, Worthington) and dissociator (Miltenyi Biotec, #130-092-235). The astrocyte and microglia were separated by anti-ACSA-2 micro beads (130-097-679, Miltenyi Biotec) and anti-CD11b micro beads (130-049-601, Miltenyi Biotec), respectively. Then, the cell suspension was then incubated with anti-O4 micro beads (130-094-543, Miltenyi Biotec) for OPC purification.

Rodent primary culture of oligodendrocyte progenitor cells (OPCs) and differentiation: Primary mouse OPCs were isolated from cortices of pups from P0 to P2 using immunopanning procedure as described previously (Hammond et al., 2015; Zhang et al., 2020; Zhang et al., 2018b). Cerebral cortices were enzymatically digested using papain (20 U/ml, #LK003176, Worthington) supplemented with DNase I (250 U/ml; #D5025, Sigma) and D-(+)-glucose (0.36%;

#0188 AMRESCO) and mechanically triturated to obtain single cell suspension. The mixed glial cells were plated on poly-D-lysine (PDL, #A003-E, Millipore) coated 10 cm dishes and cultured in DMEM medium (#1196092, Thermo Fisher) with 10% heat-inactivated fetal bovine serum (#12306-C, Sigma) and penicillin/streptomycin (P/S, #15140122, Thermo Fisher). After 24 hours incubation, cells were washed using HBSS (with calcium and magnesium, #24020117, Thermo Fisher), and cultured in serum-free growth medium (GM), containing 30% of B104 neuroblastoma medium and 70% of N1 medium (DMEM with 5 µg/ml insulin (#I6634, Sigma), 50 µg/ml apo-transferrin (#T2036, Sigma), 100 µM putrescine (#P5780, Sigma), 30 nM Sodium selenite (#S5261, Sigma), 20 nM progesterone (#P0130, Sigma)) until 80% of cellular confluency. The cells were then dissociated in single cell suspension and seeded to Thy1.2 (CD90.2) antibody (#105302, Biolegend) coated Petri-dish to deplete astrocytes, neurons and meningeal cells followed by incubation on NG2 antibody (#AB5320, Millipore) coated Petri-dish to select OPCs. OPCs were then cultured on PDL-coated plates with GM plus 5 ng/ml FGF (#450-33, Peprotech), 4 ng/ml PDGF-AA (#315-17, Peprotech), 50 µM Forskolin (#6652995, Peprotech,) and glutamax (#35050, Thermo Fisher). OPCs were differentiated in the differentiation medium, consisting of F12/high-glucose DMEM (#11330032, Thermo Fisher Scientific) plus 12.5 µg/ml insulin, 100 µM Putrescine, 24 nM Sodium selenite, 10 nM Progesterone, 10 ng/ml Biotin, 50 µg/ml Transferrin (#T8158, Sigma), 30 ng/ml 3,3′,5-Triiodo-L-thyronine (#T5516, Sigma), 40 ng/ml L-Thyroxine (#T0397, Sigma-Aldrich), glutamax and P/S.

Vector-mediated TCF7l2 expression in primary oligodendrocytes and Oli-Neu cells: The expression vectors pFlag-CMV2-TCF7l2-E2, pFlag-CMV2-TCF7l2-S2, and pFlag-CMV2-TCF7l2-M1 were provided by Dr. Andreas Hecht at the University of Freiburg, Germany and were described in the original publication (Weise et al., 2010). For vector-mediated TCF7l2 overexpression in primary OPCs or Oli-Neu cells, the transfection was conducted by FuGENE6 kit (Cat#2619, Promega) according to the manufacturer's protocol.

Enzyme-linked immunosorbent assay (ELISA): The medium collected from primary culture were used for BMP4 measurement assay at day 2 of differentiation. The BMP4 concentration was determined using the BMP4 ELISA kit (Cat#OKEH02960, Aviva System Biology). ELISA was performed according to our previous protocol (Zhang et al., 2020).

Chromatin immunoprecipitation (ChIP): ChIP assays were performed using a SimpleChIP Enzymatic Chromatin IP kit (#9003; Cell Signaling Technologies). Briefly, cells were cross-linked using 37% formaldehyde at a final concentration of 1% for 10 min at room temperature

and then quenched with 125 mM glycine for 5 min. Cells were washed twice with cold PBS, harvested in PBS with protease inhibitor cocktail (PIC) and lysed to get nuclei. Chromatin was harvested, fragmented using micrococcal nuclease to length of approximately150-900 bp and then briefly sonicated to lyse nuclear membranes. The digested chromatin (500 µg) was subjected to immunoprecipitation with specific TCF7L2 antibody (Celling Signaling) or anti-Rabbit IgG (#2729 Cell signaling) as negative control overnight at 4° C with rotation and followed by ChIP-Grade protein G magnetic beads and incubation for 2 hours at 4° C with rotation. After immunoprecipitation, the chromatin was eluted from the antibody/protein G magnetic beads and cross-links were reversed. DNA was purified and analyzed by PCR. Primer sequences (Integrated DNA Technologies) for the Bmp4 binding site were as follows: forward primer 5'-GGTACCTGCACTTAAGCTTTGTCGG 3′, and Reverse primer: 5'-TCGTAGTCGCTGCACGCAG-3′. The data were quantified by percent input and performed in triplicates.

Protein extraction and Western blot assay: Protein extraction and Western blot assay were performed as previously described with modifications (Wang et al., 2016; Zhang et al., 2020). Tissue or cells were lysed using N-PER™ Neuronal Protein Extraction Reagent (#87792, Thermo Fisher) supplied with protease inhibitor cocktail (#5871S, Cell Signaling Technology) and PMSF (#8553S, Cell Signaling Technology) on ice for 10 min and centrifuged at 10,000 × g for 10 min at 4°C to pellet the cell debris. Supernatant was collected for concentration assay using BCA protein assay kit (#23225, Thermo Fisher Scientific). Protein lysates (30 µg) were separated by AnykD Mini-PROTEAN TGX precast gels (#456-9035, BIO-RAD) or 7.5% Mini-PROTEAN TGX precast gels (#456-8024, BIO-RAD). The proteins were then transferred onto 0.2 µm nitrocellulose membrane (#1704158, BIO-RAD) using Trans-blot Turbo Transfer system (#1704150, BIO-RAD). The membranes were blocked with 5% BSA (#9998, Cell signaling) for 1 hour at room temperature and incubated with primary antibodies at overnight 4 °C, followed by suitable HRP-conjugated secondary antibodies. Proteins of interest were detected using Western Lightening Plus ECL (NEL103001EA, Perkin Elmer). NIH Image J was used to quantify protein levels by analyzing the scanned grey-scale films. Primary and secondary antibodies used were: TCF7l2 (1:1000, #2569S, Cell Signaling Technology), MBP (1:1000, #NB600-717, Novus), CNPase (1:1000, #2986, Cell Signaling Technology), HDAC2 (1:1000, #5113P, Cell Signaling Technology), TLE3 (1:1000, #11372-1-AP, Proteintech), β-actin (1:1000, #4967L, Cell Signaling Technology), GAPDH (1:1000, #2118L, Cell Signaling Technology), and HRP goat anti-rabbit (1:3000, 31460, #AB_228341, Thermo Fisher Scientific), anti-mouse (1:3000, #31430,

#AB_228307, Thermo Fisher Scientific) or anti-rat (1:3000, #7077, Cell Signaling Technology) secondary antibodies.

Protein co-immunoprecipitation (Co-IP): Co-IP was performed as previously described with some modifications (Lang et al., 2013; Wang et al., 2017). Proteins were extracted by Pierce IP Lysis/Wash Buffer (#87787, Thermo Fisher) and protein concentration was evaluated using BCA protein assay kit. 1 mg of proteins were incubated with TCF7l2 antibody (#2569S, Cell Signaling Technology) or Normal Rabbit IgG (#2729, Cell Signaling Technology) as negative control for immunoprecipitation overnight at 4°C. Pierce Protein A/G Magnetic Beads (#88802, Thermo Fisher) were washed three times with Pierce IP Lysis/Wash Buffer and added to antigen/antibody complex for 1 hour at room temperature. Beads were then washed twice with IP Lysis/Wash Buffer and once with purified water. The antigen/antibody complex was eluted from beads by boiling in Lane Marker Sample Buffer (#39001, Thermo Fisher) containing β-mercaptoethanol for SDS-PAGE and Western blotting.

RNA extraction, cDNA preparation, and RT-qPCR assay: Total RNA was isolated by RNeasy Lipid Tissue Mini Kit (#74804, QIAGEN) with on-column DNase I digestion to remove genomic DNA using RNase-Free DNase Set (#79254, QIAGEN). The concentration of RNA was determined by Nanodrop 2000. cDNA was synthesized by Qiagen Omniscript RT Kit (#205111, Qiagen). RT-qPCR was performed by using QuantiTect SYBR® Green PCR Kit (#204145, QIAGEN) on Agilent MP3005P thermocycler. The relative mRNA level of indicated genes was normalized to that of the internal control gene Hsp90 (Hsp90ab1), using the equation 2^(Ct(cycle threshold) of Hsp90 − Ct of indicated genes) according to our previous protocol (Hull et al., 2020). The gene expression levels in control groups were normalized to 1. The qPCR primers used in this study were *Sox10* (F: ACACCTTGGGACAC GGTTTTC, R: TAGGTCTTGTTCCTCGGCCAT),
Enpp6 (F: CAGAGAGATTGTGA ACAGAGGC, R: CCGATCATCTGGTGGACCT),
Mbp (F: GGCGGTGACAGACT CCAAG, R: GAAGCTCGTCGGACTCTGAG),
Plp (F: GTTCCAGAGGCCAACATCAAG, R: CTTGTCGGGATGTCCTAGCC)
Mog (F: AGCTGCTT CCTCTCCCTTCTC, R: ACTAAAGCCCGGATGGGATA C),
Myrf (F: CAGACCCAGGTGCTACAC, R: TCCTGCTTGATCATTCCGTTC),
Bmp4: (F: TTCCTGGTAACCGAATGCTGA, R: CCTGAATCTCGGCGACTTTTT),
Tcf7l2 (F: GGAGGAGAAGAACTCGGAAAA, R: ATCGGAGG AGCTGTTTTGATT),
Axin2 (F: AACCTATGCCCGTTTCCTCTA, R: GAGTGTAAAGACTTGGTCCACC),

Naked1 (F: CAGCTTGCTGCATACCATCTAT, R: GTTGAAAAGGACGCTCCTCTTA),
Sp5 (F: GTACTTGCCATCGAGGTAG, R: GGCTCGGACTTTGGAATC),
Gfap (GTGTCAGAAGGCCACCTCAAG/ CGAGTCCTTAATGACCTCACCAT),
Slc1a2 *(*CAACGGAGGATATCAGTCTGC/ TGTTGGGAGTCAATGGTGTC*),*
Id1 (F: CTCAGGATCATGAAGGTCGC, R: AGACTCCGAGTTCAGCTCCA),
Id2 (F: ATGGAAATCCTGCAGCACGTC, R: TGGTTCTGTCCAGGTCTCT),
*Id3 (*CGACCGAGGAGCCTCTTAG/ GCAGGATTTCCACCTGGCTA*),*
*Id4 (*CAGTGCGATATGAACGACTGC/ GACTTTCTTGTTGGGCGGGAT),
Hsp90 (F: AAACAAGGAGATTT TCCTCCGC, R: CCGTCAGGCTCTCATATCGAAT).

cRNA probe preparation, mRNA in situ hybridization (ISH), and combined mRNA ISH and immunohistochemistry (ISH/IHC): Probe preparation, mRNA in situ hybridization, and combination of ISH/IHC were performed by using the protocols in our previous studies (Hammond et al., 2015; Zhang et al., 2020). In brief, we used a PCR-based approach to amplify 907bp and 623bp fragments of *Bmp4* and *Mag* mRNA, respectively. The primer sets we used were: Bmp4-forward: 5'-CCTGCAGCGATCCAGTCT-3'/ Bmp4-reverse: 5'-GCCCAATCTCCACTCCCT-3'; Mag-forward: 5'-CAAGAGCCTCTACCTGGATCTG-3'/Mag-reverse: 5'-AGGTTCCTGGAGGTACAAATGA-3'. The core sequence (GCGATTTAGGTGACACTATAG) recognized by SP6 RNA Polymerase was attached to the 5' of the reverse primers. The core sequence (GCGTAATACGACTCACTATAGGG) recognized by T7 RNA Polymerase was attached to the 5' of the forward primers. The resulting PCR products were purified and used as templates for in vitro transcription by employing DIG RNA Labeling Kit (SP6/T7) (Roche #11175025910). The resulting RNAs generated from SP6-mediated in vitro transcription were used as positive probes (cRNA, complementary to the target mRNAs) whereas those generated from T7-mediated in vitro transcription were used as negative probes (same sequence as the target mRNA). Frozen sections (12μm thick) were used for mRNA ISH. Hybridization was performed in a humidity chamber at 65^0C for 12 – 18 hours, followed by a series of stringent washing by saline-sodium citrate (SSC) buffer at 65^0C (2x SSC 20 min for 3 times and then 0.2x SSC 20 min for 3 times) and RNase digestion at 37^0C (30 min) to eliminate non-specific binding and non-hybridized mRNAs. The DIG signals were visualized by NBT/BCIP method (Roche, #11697471001). Depending on the abundance of target mRNAs, the duration of NBT/BCIP incubation (at 4^0C) ranged from 4 hours to overnight.
For combined ISH/IHC, frozen sections (12μm thick) were used. DIG-conjugated cRNA probe hybridization was performed according to the procedure described above. After a series post-

hybridization SSC washing and RNase digestion, the sections was briefly rinsed in TS7.5 buffer (0.1M Tris-HCl, 0.15M NaCl, pH7.5) followed by incubation in 1% blocking reagent (prepared in TS7.5 buffer) (Roche #11096176001) for 1 hr at room temperature. After blocking, a cocktail of anti-Sox10 antibody (1:100, #AF2864, R&D Systems) and AP-conjugated anti-DIG antibody (Roche #11093274910) diluted in 1% blocking reagent was applied and incubated at 4^0C for overnight. After antibody incubation, the sections were washed in TNT buffer (TS7.5 + 0.05% Tween-20) 10 min for 3 times. The primary antibody of Sox10 was visualized by incubating Alexa Fluor 488-conjugated secondary antibody at room temperature for 1 hr. The DIG-conjugated mRNA signals were visualized by HNPP/Fast Red Fluorescent Detection set (Roche #11758888001) according to the kit instructions.

Tissue preparation and immunohistochemistry (IHC): Tissue preparation and IHC were conducted as previously described (Hammond et al., 2015; Zhang et al., 2020; Zhang et al., 2018b). Mice were perfused with ice-cold PBS (pH = 7.0, Catalog #BP399-20, Fisher Chemical), and post-fixed in fresh prepared 4% paraformaldehyde (PFA, Catalog #1570-S, Electron Microscopy Science, PA) at room temperature for 2 hours. Tissues were washed three times (15 min per each time) using ice-cold PBS and cryoprotected using 30% sucrose (#S5-3, Fisher Chemical) in PBS at 4°C overnight followed by embedding in OCT prior. Twelve microns thick sections were serially collected and stored in −80 °C. For immunohistochemistry, slice was air dry in room temperature for at least 1 hour, and blocked with 10% Donkey serum in 0.1% Triton X-100/PBS (v/v) for 1 hour at room temperature. Tissue was incubated with primary antibodies overnight at 4°C, washed three times in PBST (PBS with 0.1% Tween-20), and incubated with secondary antibodies at room temperature for 2 hours. DAPI was applied as nuclear counterstain. All images shown were obtained by Nikon C1 confocal microscope. An optical thickness of 10 μm was used for confocal z-stack imaging (step size 1 μm and 11 optical slices), and the maximal projection of the z-stack images was used for data quantification. Primary antibodies included Sox10 (1:100, #AF2864, R&D Systems), Sox10 (1:100, #ab155279, Abcam), HDAC2 (1:100, #5113P, Cell Signaling Technology), TCF7l2 (1:100, #2569S, Cell Signaling Technology), β-catenin (Cat#7202,RRID:AB_476865,1:200, Sigma), P-Smad 1/5 (Cat#9516, RRID:AB_491015,1:200, Cell Signaling Technology), CC1 (1:100, #OP80, Millipore), PDFGRα (1:100, #AF1062, R&D Systems), APC(sc-896,RRID: AB_2057493, 1:100,Santa Cruz Biotechnology), BLBP (1:100, #ABN14, Millipore), Sox9 (RRID:AB_2194160,1:200, R&D system, AF3075). All species-specific secondary antibodies (1:500) were obtained from Jackson ImmunoResearch.

Immunocytochemistry (ICC): Primary cells attached to the coverslips were fixed in 4% PFA for 15 min followed by rinse with PBS. The immunocytochemistry was performed as our previous studies (Guo et al., 2012; Hammond et al., 2015; Zhang et al., 2020). The following antibodies were used in our study: Sox10 (RRID: AB_2195374,1:100,Santa Cruz Biotechnology, sc-17342; RRID: AB_778021, 1:500, Abcam, ab27655), Mbp (RRID:AB_2564741, 1:500, Biolegend, SMI-99), TCF7l2 (2569S, RRID:AB_2199826, 1:200, Cell Signaling Technology), P-Smad 1/5 (Cat#9516, RRID:AB_491015,1:200, Cell Signaling Technology).

Gene clone and luciferase activity assay: To generate a luciferase reporter under the control of the *intronic* promoter of mouse Bmp4 gene, a 439-bp DNA fragment containing the *Bmp4* promoter was amplified using the spinal cord genomic DNA with the forward primer 5'-GGTACCTGCACTTAAG***CTTTG***TCGG -3' (underlined sequence is KpnI site, bold italic sequence is TCF7l2 binding site) and the reverse primer 5'-CTCGAGACGGAATGGCTCCTAAAATG-3' (underlined sequence is XhoI site). The PCR product was cloned into pGEM-T-Easy vector and confirmed by DNA sequencing. After digesting with KpnI and XhoI, the fragment was cloned into pGL2-Basic vector. The resulting luciferase reporter was designated as pGL2-Bmp4-Luc. Using pGL2-Bmp4-Luc as a template, TCF7l2-binding mutation constructs were generated by PCR using the above reverse primer and the following forward primer: GGTACCTGCACTTAAGTGGTGTCGG (underlined sequence is Kpn I site). The resulting mutated luciferase reporter was designated as pGL2-mBmp4-Luc. The dual luciferase assay was done in triplicate using TD-20/20Luminometer (Promega) according to the manufacturer's instructions. Briefly, 0.25 μg of a luciferase reporter (Bmp4-Luc or mutBmp4-Luc), 0.25 μg of TCF7l2-S2 or TCF7l2-E2, and 5 ng of Renilla luciferase report (Promega) were co-transfected into U87 human primary glioblastma cells by using ESCORT V transfection reagent (Sigma). The fold increase in relative luciferase activity is a product of the luciferase activity induced by TCF7l2-S2 or TCF7l2-E2 (backbone vector pCMV) divided by that induced by an empty pCMV vector.

Experimental designs and statistical analyses: All quantification was conducted by lab members blinded to genotypes or treatments. For in vivo gene cKO studies, animals were derived from multiple litters. Data were presented as mean ± standard error of mean (s.e. m.) throughout this manuscript. We used bar graph and scatter dot plots to show the distribution of the data. Each dot (circle, square, or triangle, if applicable) in the scatter dot plots represents

one mouse or one independent experiment. We used Shapiro–Wilk approach was used for testing data normality. F test and Browne–Forsythe test were used to compare the equality of variances of two and three or more groups, respectively. The statistical analysis details of Figs. 1-3 were summarized in Table 1. P values of t test were displayed in each graph. Welch's correction was used for Student's t test if the variances of two groups were unequal. For comparisons among three or more groups with equal variances, ordinary one-way ANOVA was used followed by Tukey's multiple comparisons, otherwise Welch's ANOVA was used followed by unpaired t test with Welch's correction. All data plotting and statistical analyses were performed using GraphPad Prism version 8.0. P value less than 0.05 was considered as significant, whereas greater than 0.05 was assigned as not significant (ns).

Results:

BMP4 is expressed primarily in oligodendroglial lineage

BMP4 is a secreted protein and the mRNA expression better reflects its cellular origin. To determine cellular source of BMP4 *in vivo*, we purified different cell populations from the brain by MACS (**Fig. 1-1 A-D**) immediately followed by mRNA quantification. We found that BMP4 was highly enriched in $O4^+$ oligodendroglial lineage (**Fig. 1A**) which consists of late post-mitotic oligodendrocyte progenitor cells (OPCs) and immature OLs (Armstrong et al., 1992). To determine BMP4 dynamics within the oligodendroglial lineage, we employed primary OPC culture and differentiation system (Zhang et al., 2018b) and demonstrated that BMP4 was low in OPCs and rapidly upregulated (by >150-fold) in differentiating OLs (**Fig. 1B**), a dynamic pattern correlated with that of TCF7l2 (**Fig. 1C**) (Hammond et al., 2015), suggesting a potential link between BMP4 and TCF7l2 during OL differentiation.

TCF7l2 deletion upregulates BMP4 and activates canonical BMP4 signaling *in vivo*

Our prior study reported an upregulation of BMP4 in the CNS of TCF7l2 cKO mutants (Hammond et al., 2015). To determine the regulation of BMP4 at the cellular level, we deleted TCF7l2 in the oligodendroglial lineage using time-conditioned Olig2-CreER^{T2} and assessed BMP4 expression *in vivo* 24 hours after tamoxifen treatment (**Fig. 1D**). During this short time window, TCF7l2 deletion-elicited OL differentiation defect (Hammond et al., 2015; Zhao et al., 2016) was barely seen, as indicated by similar signals of mRNA in situ hybridization (ISH) for the mature OL marker MAG (**Fig. 1E**). We found a significant increase of *Bmp4* mRNA in TCF7l2 cKO spinal cord demonstrated by qPCR (**Fig. 1F**) and confirmed by ISH (**Fig. 1G**). Combined ISH and immunohistochemistry (IHC) showed that BMP4 was upregulated in $Sox10^+$

cells in the spinal cord of TCF7l2 cKO mice (**Fig. 1H**), indicating that TCF7l2 controls oligodendroglial BMP4 expression *in vivo*.

BMP4 activates canonical BMP signaling through phosphorylating SMAD1/5 (Retting et al., 2009), thus the phosphorylated form of SMAD1/5 (p-SMAD1/5) is a reliable surrogate for the signaling activation. We next used IHC antibodies specifically recognizes p-SMAD1/5 to assess BMP signaling activation at the cellular level. We found that p-SMAD1/5 was primarily observed in Sox10-negative cells, presumably astroglial lineage cells in non-Cre Ctrl mice (**Fig. 1I**, arrows) and, in contrast, upregulated in Sox10-expressing oligodendroglial lineage cells (**Fig. 1I**, arrowheads) in TCF7l2 cKO mice. Furthermore, the expression of the canonical BMP signaling target genes *Id1, Id2*, and *Id3* was significantly elevated in TCF7l2 cKO mice (**Fig. 1J**). The upregulation of BMP4 and the signaling activity were confirmed in the brain by an independent *Plp1-CreER*^{T2}, *Tcf7l2*$^{fl/fl}$ mutant mice (**Fig. 1K**), suggesting that TCF7l2 controls BMP4 and the canonical BMP4 signaling activity in an autocrine manner not only in the spinal cord but also in the brain.

BMP4 enhances astrocyte generation at the expense of oligodendrogenesis (Gomes et al., 2003; Grinspan, 2020; Wu et al., 2012). To determine the effect of TCF7l2 cKO-elicited BMP4 upregulation on astrocyte development, we quantified astrocyte density *in vivo*. No significant difference was observed in the number of Sox9$^+$BLBP$^+$ or Sox9$^+$S100β$^+$ astrocytes (**Fig. 1-2 A-D**), nor the expression of mature astrocyte markers GFAP and GLT-1 (**Fig. 1-2 E-F**) between non-Cre Ctrl and TCF7l2 cKO. Collectively, our data demonstrate that the Wnt effector TCF7l2 represses BMP4 expression and controls autocrine BMP signaling activity during OL differentiation.

TCF7l2 directly represses BMP4 transcription

A repressive role of TCF7l2 in oligodendroglial lineage has not been reported. Bioinformatic analysis showed that the intronic promoter of the mouse *Bmp4* gene (Thompson et al., 2003) contained a DNA binding motif of TCF7l2 (**Fig. 2A**). Chromatin immunoprecipitation (ChIP) followed by qPCR (ChIP-qPCR) confirmed the physical binding of TCF7l2 to this regulatory element (**Fig. 2B**). To determine the functional output of TCF7l2 binding, we sought to analyze *Bmp4* promoter-driven luciferase activity. We showed that oligodendroglial lineage cells expressed TCF7l2 E isoform (~79kD) and M/S isoforms (~58kD) in the spinal cord (**Fig. 2-1 A, B**) and in primary brain OLs (Hammond et al., 2015). We therefore tested the effect of the representative isoform (E2 and S2) (Weise et al., 2010) (**Fig. 2-1 C**) on *Bmp4* transcription activity. To this end, we cloned a 439-bp intronic promoter sequence (Thompson et al., 2003)

into the luciferase reporter pGL2 vector and co-transduced with TCF7l2-E2 or S2 vectors into U87, a human primary glioblastoma cell line. Our results demonstrated that both E2 and S2 isoforms inhibited *Bmp4*-luciferase activity (**Fig. 2C, D**). Importantly, mutation of the TCF7l2 binding site abolished the repressive effect (**Fig. 2C, D**), suggesting that TCF7l2 directly represses BMP4 expression at the transcriptional level.

TCF7l2 harbors several functional domains including a β-catenin-binding domain, a Groucho/TLE-binding domain, and a high mobility group (HMG) box DNA-binding domain (Weise et al., 2010) which specifically recognizes CTTTG DNA motif on target genes (Hatzis et al., 2008). The gene regulation (activation or repression) by TCF7l2 is determined by its interacting co-activators or co-repressors in a cell type-dependent manner (Hurlstone and Clevers, 2002). To gain mechanistic insights into how TCF7l2 inhibits BMP4, we assessed the interaction of TCF7l2 with β-catenin and histone deacetylase 2 (HDAC2) *in vivo*, both of which have been shown to compete for TCF7l2 binding (Ye et al., 2009). TCF7l2 was histologically co-labeled with HDAC2 (**Fig. 2F**) but not β-catenin (**Fig. 2E,** cf **Fig. 2-2 B2**). Co-IP followed by Western blot demonstrated that TCF7l2 bound primarily to HDAC2 yet minimally to β-catenin (**Fig. 2H**). The binding of the co-activator β-catenin to TCF7l2 displaces the co-repressor Groucho/TLE from TCF7l2 (Clevers, 2006). The co-localization and interaction of TLE3 with TCF7l2 (**Fig. 2G, H**) also supported a minimal β-catenin binding to TCF7l2 under physiological conditions. To determine the involvement of HDAC2 in TCF7l2-mediated BMP4 repression, we treated primary OLs with Trichostatin A (TSA), a pan-HDAC inhibitor (**Fig. 2-2 A1**). Consistent with previous data (Marin-Husstege et al., 2002; Ye et al., 2009), TSA decreased OL differentiation, evidenced by reduced expression of the myelin protein gene *Plp* (**Fig. 2-2 A2**). Interestingly, *Bmp4* and the canonical BMP4 signaling target *Id2* were significantly upregulated in TSA-treated OL culture (**Fig. 2I**), suggesting that the deacetylating activity of HDAC2 is required for TCF7l2-mediated BMP4 repression.

To determine whether “enforced” binding of β-catenin plays a role in TCF7l2-mediated BMP4 repression, we overexpressed Wnt3a, a typical canonical Wnt ligand, in primary OLs (**Fig. 2-2 B1**). In sharp contrast to cytoplasmic β-catenin in the control condition (**Fig. 2-2 B2**), Wnt3a expression resulted in β-catenin localization in TCF7l2^{+}DAPI^{+} nuclei (**Fig. 2-2 B2**) and led to Wnt/β-catenin activation, as evidenced by the elevation in the canonical Wnt targets *Axin2* and *Naked1* (**Fig. 2-2 B3**). However, Wnt3a expression did not perturb the expression of BMP4 and the canonical BMP4 signaling targets *Id2* and *Id4* (**Fig. 2-2 B4**). Together, these data suggest that TCF7l2 inhibits BMP4 expression through recruiting the repressive co-factors HDAC2 and

TLE3 to *Bmp4* cis-regulatory element and that β-catenin plays a dispensable role in TCF7l2-mediated BMP4 repression.

TCF7l2 promotes OL differentiation by repressing BMP4 *in vitro*

To determine the biological significance of TCF7l2 in repressing BMP4, we overexpressed TCF7l2 in primary OLs and analyzed OL differentiation (**Fig. 2-2 C1-C3**). TCF7l2 expression remarkably elevated the density of $MBP^{+}Sox10^{+}$ OLs by a greater than 2-fold (**Fig. 2J**) and significantly increased the expression of myelin protein genes (*Mbp, Plp*, and *Mog*), newly differentiated OL marker *Enpp6*, and pro-differentiation factor *Myrf* (**Fig. 2K**), indicating that TCF7l2 is sufficient for promoting OL differentiation in a cell autonomous manner. Consistent with the inhibitory role in BMP4 transcription (**Fig. 2C-D**), TCF7l2 expression reduced the amount of BMP4 protein secreted into the culture medium (**Fig. 2L**), decreased the number of $Sox10^{+}$ oligodendrocytes that were positive for p-SMAD1/5 (**Fig. 2M**), and reduced the expression of the canonical BMP4 signaling target *Id2* (**Fig. 2N**), suggesting that TCF7l2 promotes OL differentiation by inhibiting autocrine BMP4 and dampens BMP4-mediated canonical BMP/SMAD signaling activity. We did not find significant differences in the expression of the canonical Wnt target genes (Guo et al., 2015) (**Fig. 2O**), indicating that TCF7l2 plays a minor role in transcriptionally activating Wnt/β-catenin signaling in oligodendroglial lineage cells (Hammond et al., 2015). BMP4 elevated the canonical BMP/SMAD signaling activity as evidenced by Id2 upregulation upon BMP4 treatment (**Fig. 2-2 D1-D2**). We found that BMP4 abolished the upregulation of *Plp* expression elicited by TCF7l2 overexpression (**Fig. 2P**). Collectively, these data suggest that TCF7l2 promotes OL differentiation through controlling autocrine BMP4-mediated signaling.

Disrupting oligodendroglial BMP4 rescues OL differentiation defects in TCF7l2 cKO mutants

To determine the physiological significance of TCF7l2-mediated BMP4 repression on OL differentiation *in vivo*, we generated *Olig2-CreER*^{T2}, *Tcf7l2*$^{fl/fl}$ (TCF7l2 single cKO), *Olig2-CreER*^{T2}, *Tcf7l2*$^{fl/fl}$, *Bmp4*$^{fl/fl}$ (TCF7l2/BMP4 double cKO), and non-Cre Ctrl mice. In line with the above observation (**Fig. 1**), TCF7l2 disruption (**Fig. 3A-B**) caused BMP4 upregulation (**Fig. 3C**) and BMP4/SMAD signaling activation (**Fig. 3D**) in $Sox10^{+}$ oligodendroglial lineage cells (**Fig. 3E-G**) in TCF7l2 single cKO mutants. Simultaneous *Bmp4* deletion (**Fig. 3C**) normalized BMP4 signaling activity in TCF7l2/BMP4 double cKO mice (**Fig. 3D-G**).

Consistent with previous reports (Hammond et al., 2015; Zhao et al., 2016), TCF7l2 deficiency remarkably decreased the expression of myelin basic protein MBP and CNPase at

the mRNA (**Fig. 3H**) and protein level (**Fig. 3I-K**) and significantly diminished OL differentiation (**Fig. 3L-N**) in TCF7l2 single cKO mice compared with non-Cre Ctrl mice. BMP4 deletion remarkably alleviated the defects in myelin gene expression (**Fig. 3H-K**) and OL differentiation (**Fig. 3L-N**) in TCF7l2/BMP4 double cKO compared with TCF7l2 single cKO mice. Thus, our genetic results convincingly demonstrate that BMP4 dysregulation is a downstream molecular mechanism underlying OL differentiation defects elicited by TCF7l2 cKO *in vivo*.

BMP4 gain-of-function by transgenic overexpression driven by neuronal promoter inhibits OL differentiation (Gomes et al., 2003). To determine the effect of BMP4 loss-of-function on OL differentiation *in vivo*, we analyzed *Pdgfrα-CreER*^{T2}*, Bmp4*$^{fl/fl}$ (BMP4 cKO) mice and non-Cre Ctrl mice. Despite a greater than 4-fold BMP4 reduction in BMP4 cKO mice compared with non-Cre Ctrl littermate controls (**Fig. 3-1 A**), we did not find significant differences in the number of differentiated OLs and OPCs (**Fig. 3-1 B-D**), myelin gene expression (**Fig. 3-1 E**), or the rate of OL differentiation indicated by the number of APC^{+}TCF7l2^{+} (Zhang et al., 2018a) newly generated OLs (**Fig. 3-1 F-I**). These data suggest that other BMP ligands, such as BMP2 and BMP6 from other cell types (See et al., 2007), may compensate for BMP4 loss-of-function and maintained normal BMP/SMAD signaling activity and OL differentiation.

Discussion:

By employing *in vitro* primary culture and genetic mouse models in combination with biochemical and molecular analyses, we made several novel observations: 1) oligodendroglial lineage is the primary cellular source of BMP4 in the CNS; 2) TCF7l2 controls the level of autocrine BMP4 signaling activity in oligodendroglial lineage cells by transcriptionally repressing *Bmp4* gene; and 3) TCF7l2 promotes OL differentiation by dampening autocrine BMP4-mediatd signaling *in vitro* and *in vivo*.

Our previous studies have shown that TCF7l2 is transiently upregulated in newly-formed OLs (Hammond et al., 2015) that are positive for the Wnt/β-catenin negative regulator adenomatous polyposis coli (APC) (Lang et al., 2013) (**Fig. 4A**). Based on our findings, we proposed a “Wnt-independent and BMP4-dependent” role of TCF7l2 in promoting OL differentiation (**Fig. 4B**). In this working model, APC limits the nuclear availability of β-catenin for TCF7l2 binding and Wnt/β-catenin activation whereas TCF7l2 binds to the cis-regulatory elements of *Bmp4* genes and directly represses BMP4 transcription likely by recruiting co-repressors HDAC2 and TLE3, both of which lack DNA-binding domains. Disrupting the DNA-binding TCF7l2 leads to uncontrolled BMP4 expression and inhibits OL differentiation through BMP4-mediated autocrine signaling upregulation.

TCF7l2 is upregulated primarily in active MS lesions (with extensive remyelination) but minimally in chronic MS lesions (with scarce remyelination) (Fancy et al., 2009). Recent studies demonstrate an elevation of BMP4 in both active and chronic MS lesions (Costa et al., 2019; Harnisch et al., 2019) although the cell types producing BMP4 need to be defined (Grinspan, 2020). The repressive TCF7l2-BMP4 regulation suggests that augmenting TCF7l2 may have synergistic potential in dampening BMP4 signaling, which is dysregulated in chronic MS lesions (Grinspan, 2015, 2020) and in promoting OL differentiation and remyelination given the multi-modal actions of TCF7l2 in propelling OL lineage progression and maturation (Zhao et al., 2016).

The proposed working model (**Fig. 4B**) may also be applicable to a broader cell lineage. Beyond its role in CNS oligodendroglial lineage, the Wnt effector TCF7l2 regulates a spectrum of biological processes of other lineage cells, such as hepatic metabolism (Boj et al., 2012), colorectal tumorigeneis (Angus-Hill et al., 2011; Wenzel et al., 2020), adipocyte function (Chen et al., 2018), and heart development (Ye et al., 2019) where BMP signaling plays crucial roles (Brazil et al., 2015; Wang et al., 2014). The connection between TCF7l2 and autocrine BMP4 signaling has not been reported in these cell types. In this regard, our take-home message (Fig. 4B) point to a new direction for studying the crosstalk between TCF7l2 and BMP4/SMAD signaling pathways in regulating the development and function of TCF7l2-expressing and BMP/Wnt-operative cells in the body. Supporting this claim, recent data suggest that TCF7l2 overexpression downregulates *Bmp4* mRNA in a cardiac cell line (Ye et al., 2019).

In summary, our *in vitro* and *in vivo* data unravel a previously unrecognized role of the Wnt effector TCF7l2 in promoting OL differentiation by negatively controlling BMP4-mediated autocrine signaling. Given that BMP4 is dysregulated in chronic MS lesions, our findings of the biological function of TCF7l2-BMP4 connection in OL differentiation indicate that enforced TCF7l2 expression may be a potential therapeutic option in promoting OL and myelin regeneration in chronic MS lesions and animal mode.

Fig. 1 – TCF7l2 deletion activates BMP4 and BMP4-mediated signaling in oligodendroglial lineage

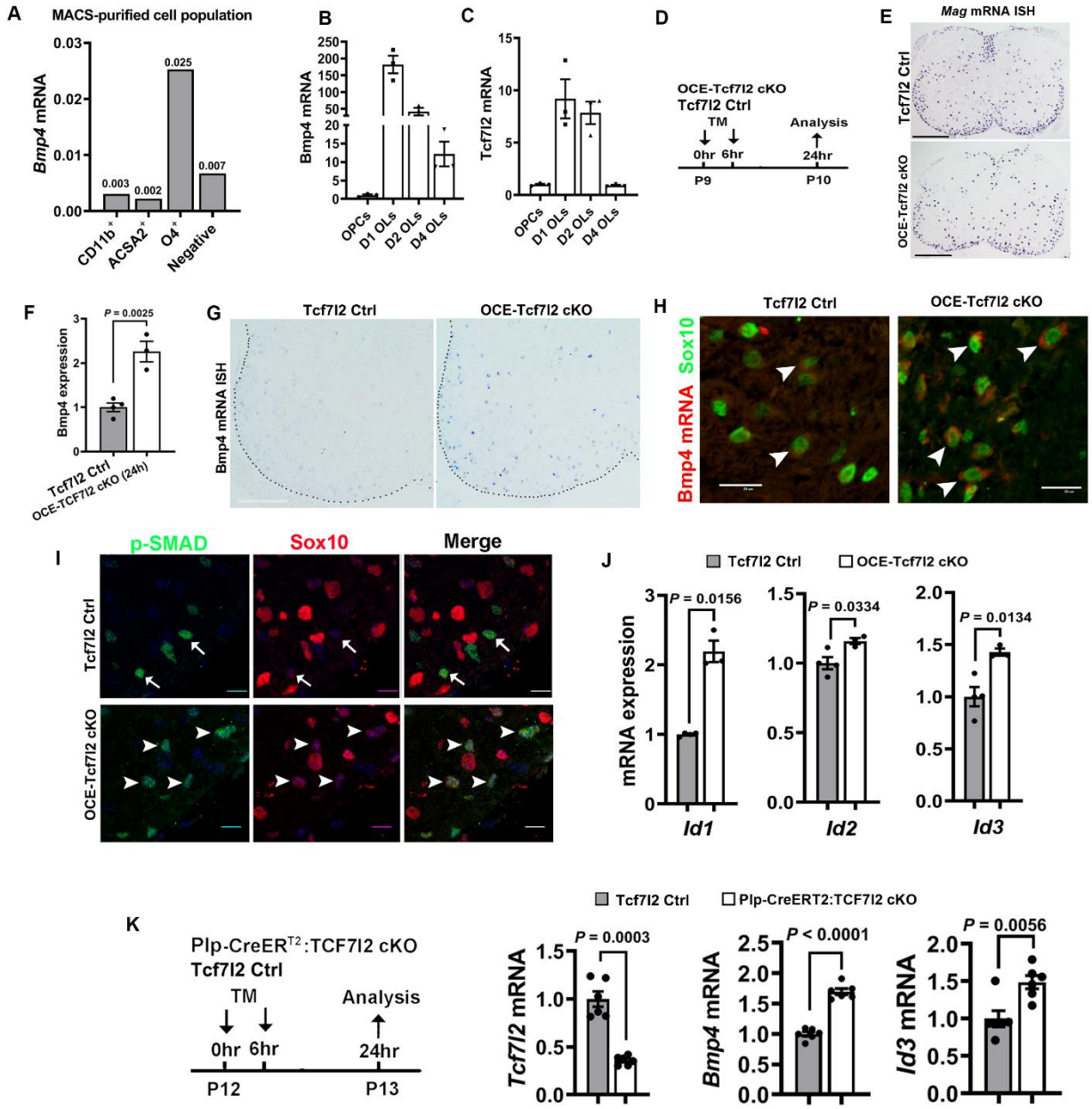

A, RT-qPCR assay for *Bmp4* in brain microglial (CD11b$^+$), astroglial (ACSA2$^+$), and oligodendroglial lineage (O4$^+$) cells at postnatal day 5 (P5) purified by MACS. Negative, CD11b/ACSA2/O4-depleted cells (three brains pooled together).

B-C, RT-qPCR assay for *Bmp4* and *Tcf7l2* mRNA in primary OPCs maintained in proliferating medium and differentiating OLs maintained in differentiation medium for 1-4 days (D1-D4 OLs). D1-D2 OLs, immature OLs; D4 OLs, mature OLs.

D, experimental design for **E-J**. OCE-Tcf7l2 cKO (*Olig2-CreER*^{T2}:*Tcf7l2*$^{fl/fl}$); Tcf7l2 Ctrl (*Tcf7l2*$^{fl/fl}$, or *Tcf7l2*$^{fl/+}$).

E, In situ hybridization (ISH) of myelin associated glycoprotein (Mag) mRNA.

F, RT-qPCR assay of *Bmp4* mRNA in the spinal cord.

G, ISH showing *Bmp4* mRNA upregulation in the spinal cord.

H, ISH of *Bmp4* mRNA and immunohistochemistry (IHC) of oligodendroglial marker Sox10 in the ventral white matter of spinal cord.

I, double IHC of phosphorylated SMAD1/5 (p-SMAD) and Sox10 in the ventral white matter of spinal cord.

J, *Id1, Id2*, and *Id3* expression quantified by RT-qPCR in the spinal cord.

K, experimental design and RT-qPCR quantification of *Tcf7l2*, *Bmp4*, and *Id3* in the brain.

Scale bars (in μm): **E**, 500; **G**, 200; **H**, 20; **I**, 10. Please see Table 1 for statistical details throughout this study.

Fig. 2 – TCF7l2 OL differentiation by repressing BMP4 transcription

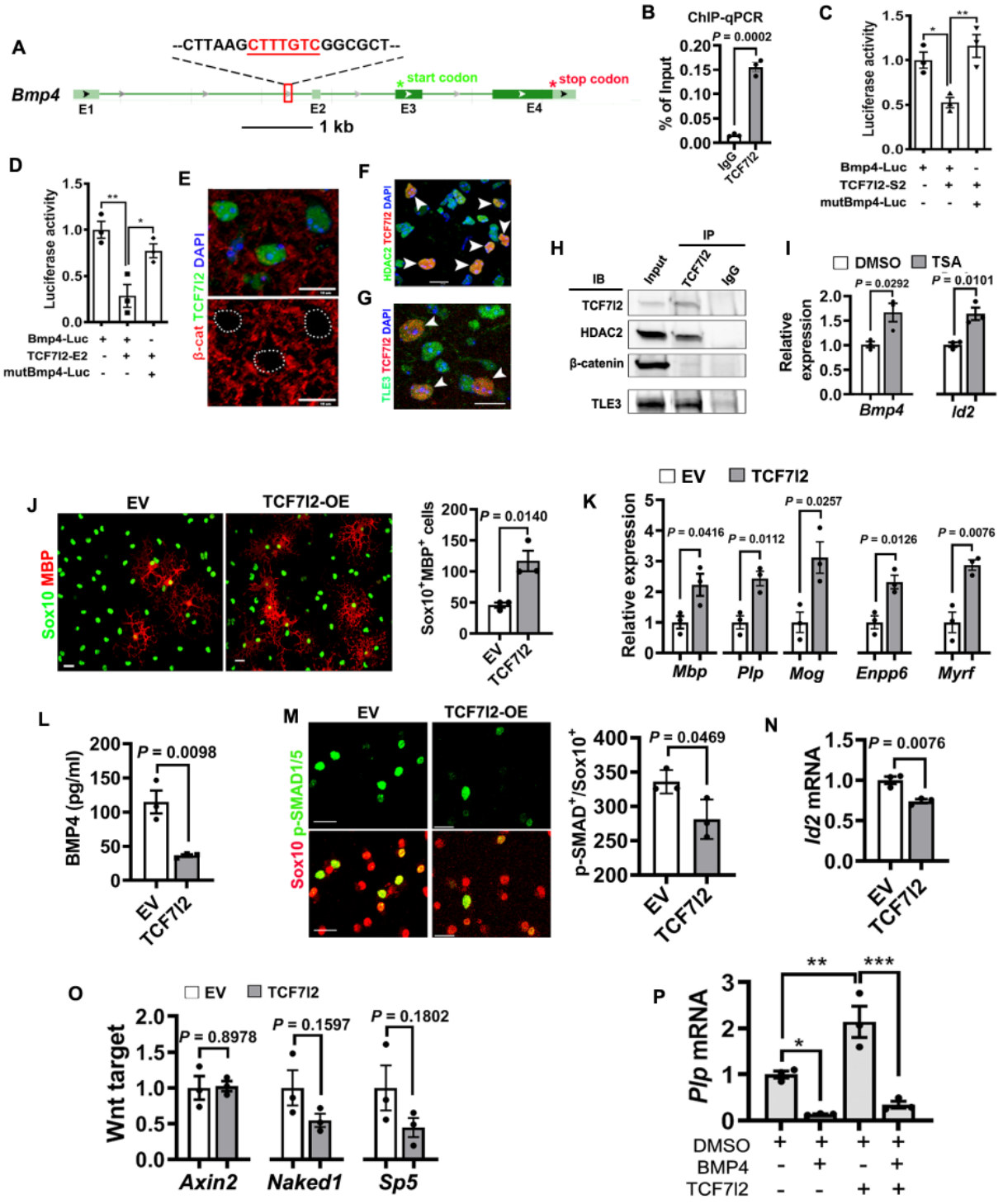

A, TCF7l2-binding site located at ~317bp upstream of the exon 2 (E2) of mouse *Bmp4* gene.

B, ChIP-qPCR of TCF7l2 binding to BMP promoter shown in **A.**

C-D, luciferase assays for Bmp4-luc and mutated Bmp4-luc (mutBmp4) in the presence of TCF7l2 S2 or E2 isoforms.

E-G, double IHC showing TCF7l2 is co-labeled with HDAC2 (**F**, arrowheads) and co-repressor TLE3 (**G**, arrowheads) but not β-catenin (**E**, dashed circles) in P7 spinal cord.

H, TCF7l2 Co-IP and Western blot detection of HDAC2, β-catenin, and TLE3 in P7 spinal cord.

I, RT-qPCR assay of *Bmp4* and *Id2* in primary OLs treated with DMSO and HDAC inhibitor TSA.

J, immunocytochemistry (ICC) and quantification of $Sox10^{+}MBP^{+}$ cells transduced with empty vector (EV) or TCF7l2-overexpression (OE) vector.

K, RT-qPCR mRNA quantification for myelin genes, newly formed OL marker Enpp6, and pro-differentiation factor Myrf.

L, ELISA assay for BMP4 concentration in culture medium.

M, representative confocal images and quantification of p-SMAD1/5 and Sox10 (#/mm^2).

N, relative mRNA of BMP4 signaling target *Id2* quantified by RT-qPCR.

O, relative expression of canonical Wnt targets quantified by RT-qPCR.

P, RT-qPCR assay for OL marker *Plp* in primary OLs treated with BMP4 and TCF7l2-expressing vector. Scale bars=10 μm except K, 20 μm.

Fig. 3 – Disrupting BMP4 rescues TCF7l2 deletion-elicited inhibition of OL differentiation *in vivo*

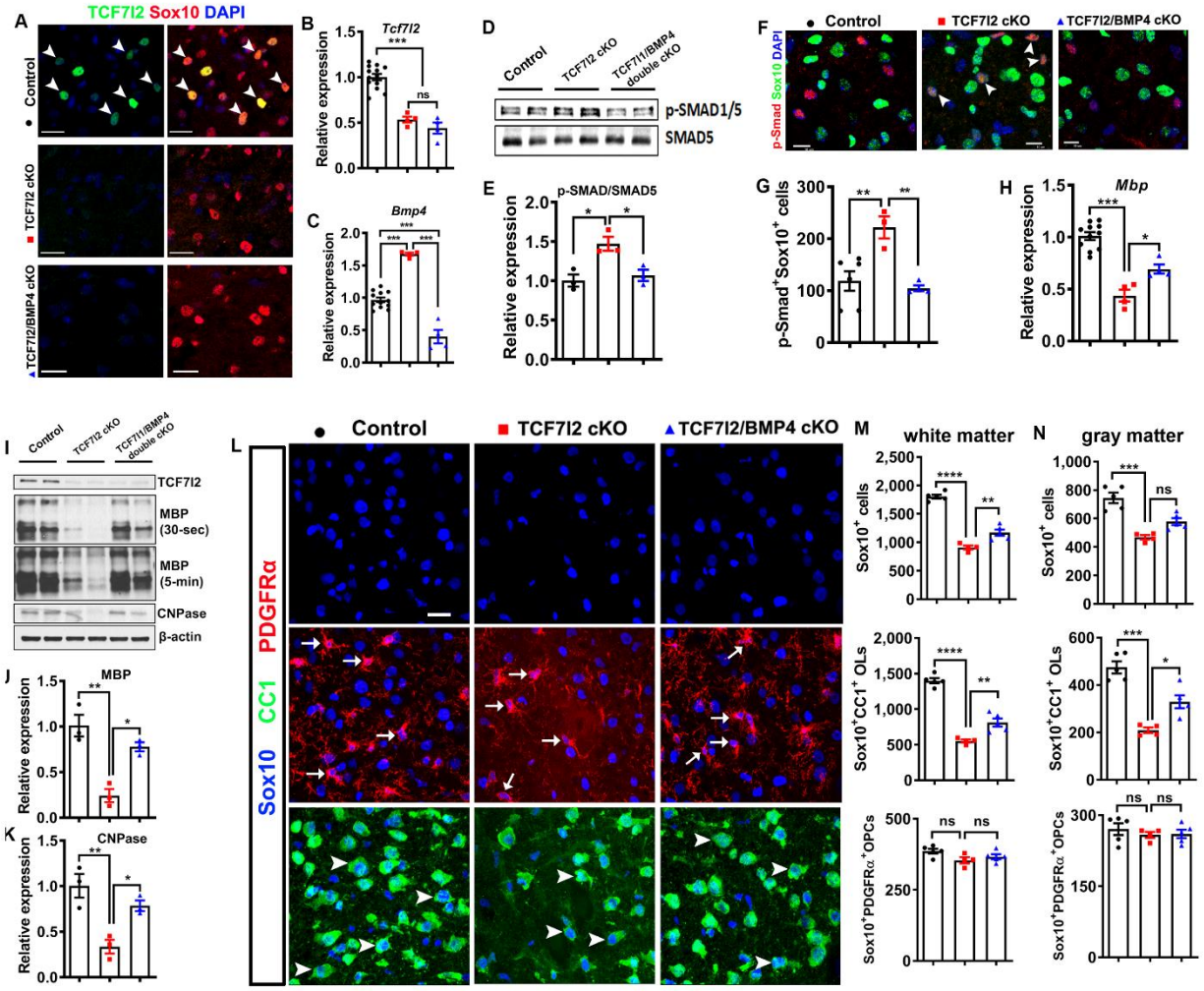

Olig2-CreER^{T2}, *Tcf7l2*$^{fl/fl}$ (TCF7l2 cKO), *Olig2-CreER*^{T2}, *Tcf7l2*$^{fl/fl}$, *Bmp4*$^{fl/fl}$ (TCF7l2/BMP4 cKO), and control mice were treated with tamoxifen at P6 and P7 and analyzed at P13.

A, representative confocal images of TCF7l2 and Sox10 co-labeling cells (arrowheads) in the spinal cord.

B-C, relative expression of *Tcf7l2* and *Bmp4* in the spinal cord assessed by RT-qPCR.

D-E, representative Western images and quantification of p-SMAD1/5 over SMAD5 in the forebrain.

F-G, representative confocal images and quantification of p-SMAD1/5 and Sox10 IHC (#/mm^2) in the spinal cord white matter.

H, relative *Mbp* expression quantified by RT-qPCR.

I-K, representative Western blot images and quantification of TCF7l2, MBP, and CNPase in the forebrain. β-actin serves as an internal loading control.

L, representative confocal images of Sox10, CC1, and PDGFRα IHC in the spinal cord white matter. Arrowheads, Sox10$^+$CC1$^+$ OLs; arrows, Sox10$^+$PDGFRα$^+$ OPCs.

M-N, densities (#/mm^2) of total Sox10$^+$ oligodendroglial lineage cells, Sox10$^+$CC1$^+$ OLs, and Sox10$^+$PDGFRα$^+$ OPCs in the white matter (**M**) and gray matter (**N**) of spinal cord.

Scale bars, 20 μm in A, 10 μm in F and L.

Fig. 4 – Conceptual framework of BMP4 repression by TCF7l2 in promoting OL differentiation

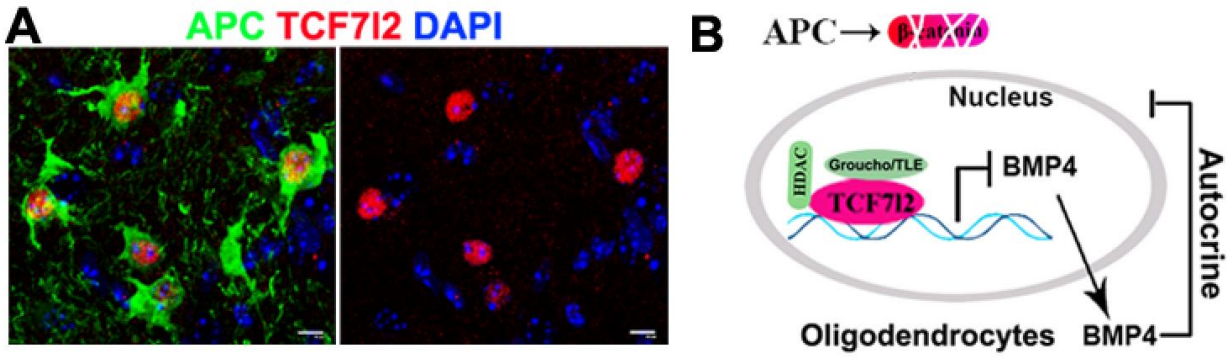

A, All TCF7l2$^+$ oligodendroglial cells are positive for APC, a negative regulator of Wnt/β-catenin signaling. **B**, proposed working model of "Wnt-independent and BMP4-dependent" role of TCF7l2 in promoting OL differentiation.

Figure 1-1: Oligodendroglial TCF7l2 deletion does not affect postnatal astrocyte maturation (related to Fig. 1)

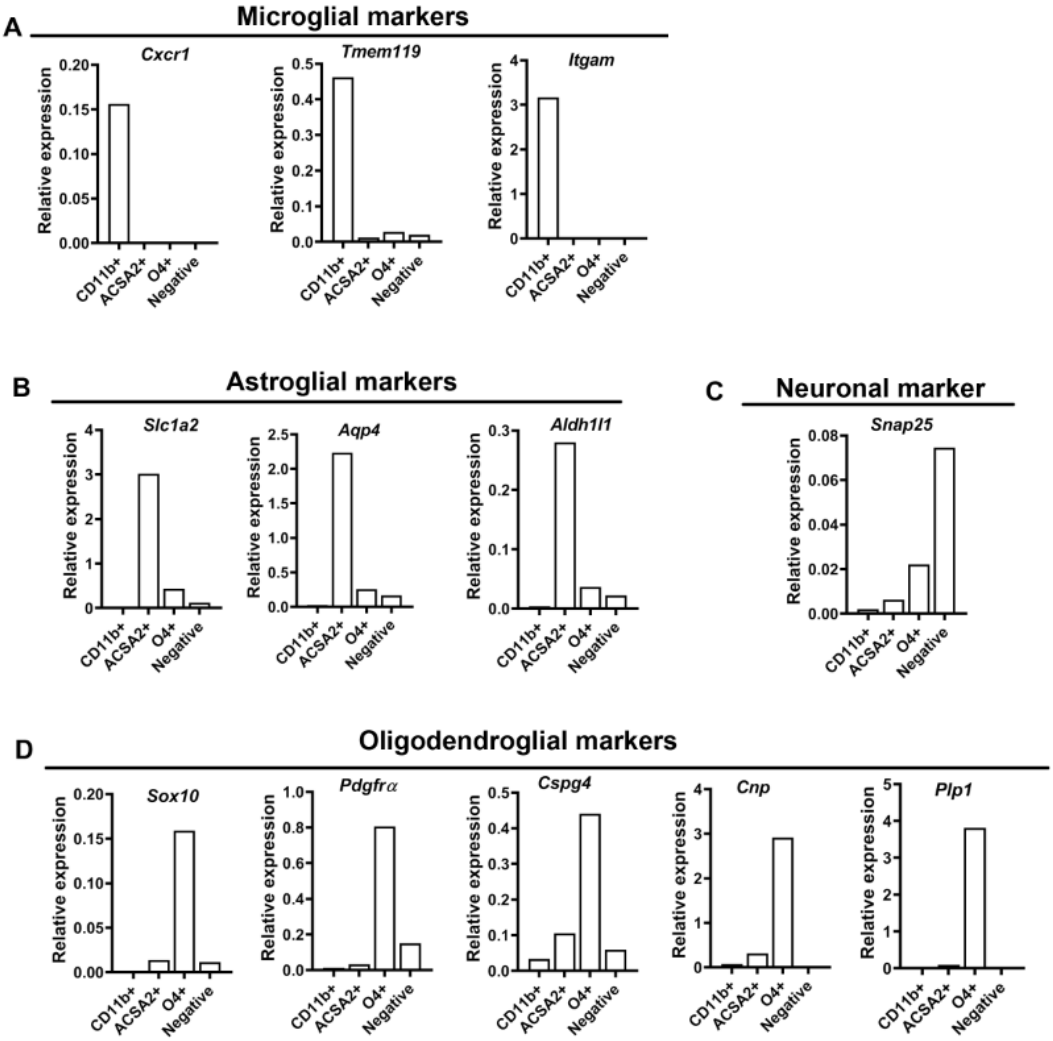

The brain of P5 C57BL/6j wild type mice (n=3, pooled together) was used for cell purification. CD11b, ACSA2 and O4-conjugated magnetic beads were used for positively selecting microglial, astroglial, and oligodendroglial lineage cells, respectively. Brain cells negative for CD11b, ACSA2, and O4 were designated as Negative components. RNA samples prepared for CD11b$^+$, ASCA2$^+$, O4$^+$, and triple negative cell populations were used for RT-qPCR assay of mRNA levels of microglial (**A**), astroglial (**B**), neuronal (**C**), and oligodendroglial (D) lineage cells. The expression of markers was normalized to that of the housekeeping gene Hsp90.

Figure 1-2: TCF7l2 deletion in Plp$^+$ oligodendroglial lineage cells activates BMP4 and BMP signaling in the brain (related to Fig. 1)

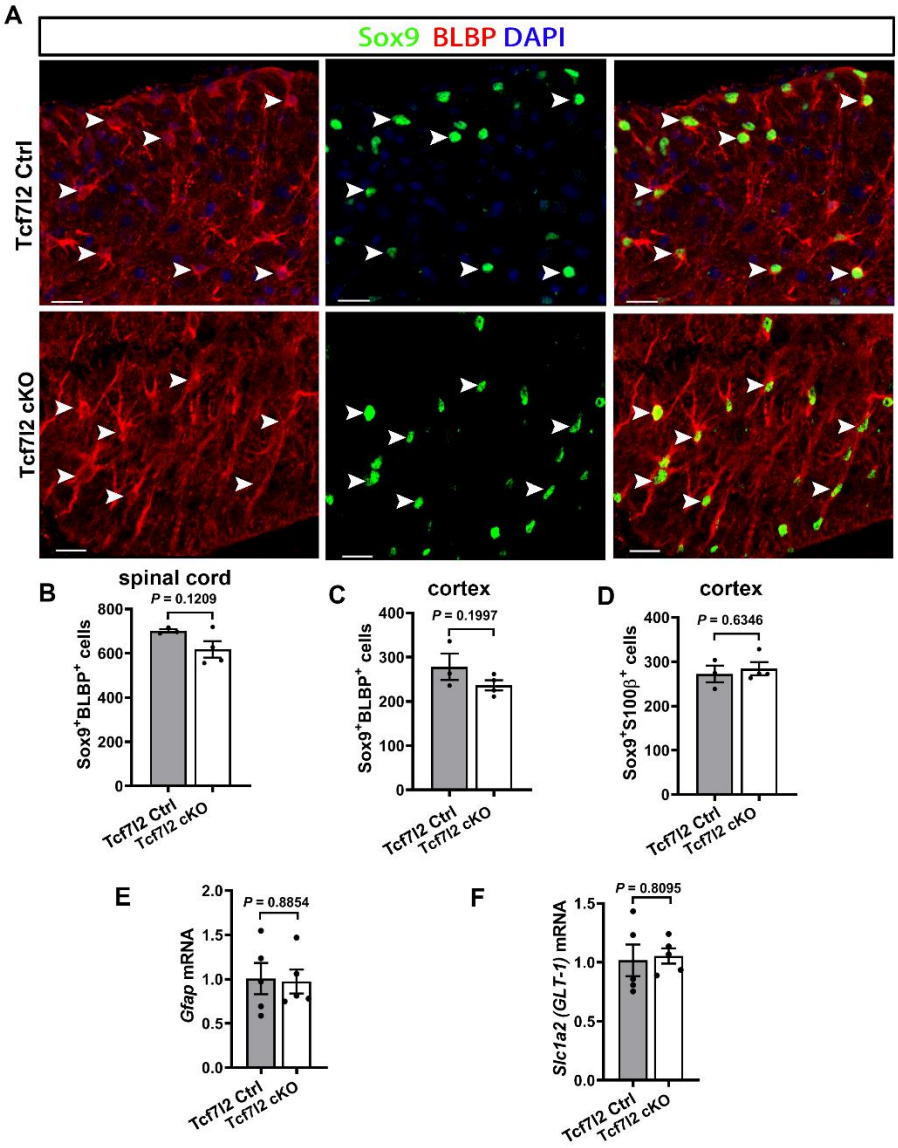

Olig2-CreER^{T2}, Tcf7l2$^{fl/fl}$ (Tcf7l2 cKO) and TCF7l2 Ctrl mice (*Tcf7l2$^{fl/fl}$*) were treated with tamoxifen at P6 and P7 and analyzed at P14. **A**, representative confocal images showing Sox9$^+$BLBP$^+$ astrocytes (arrowheads) in the spinal cord white matter. Scale bar=20μm. **B-C**, density (#/mm^2) of Sox9$^+$BLBP$^+$ astrocytes in the spinal cord white matter (**B**) and forebrain cerebral cortex (**C**).

D, Sox9$^+$S100β$^+$ astrocytes in the forebrain cerebral cortex.

E-F, RT-qPCR quantification of mature astrocyte markers *Gfap* and *Slc1a2* in the spinal cord. Two-tailed Student's *t* test, $t_{(5)}$ = 1.867 Sox9$^+$BLBP$^+$ spinal cord, $t_{(5)}$ = 1.477 Sox9$^+$BLBP$^+$ cortex, $t_{(5)}$ = 0.5057 Sox9$^+$S100β$^+$ cortex, $t_{(8)}$ = 0.1488 *Gfap*, $t_{(8)}$ = 0.2492 *Slc1a2* .

Figure 2-1: Expression of TCF7l2 isoforms in the CNS (related to Fig. 2)

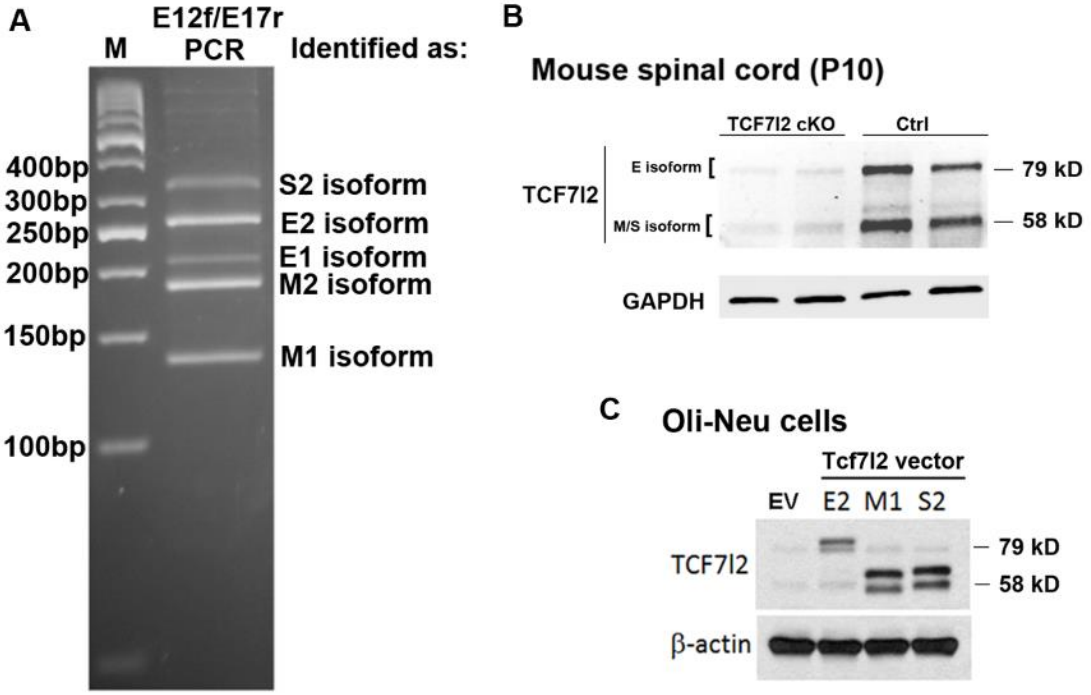

The mouse *Tcf7l2* gene has 17 exons and alternative splicing of the exons 13, 14, 15, and 16 generates E, S, and M isoforms (Weise et al., 2010).

A, PCR amplicons using the cDNA prepared from P10 mouse spinal cord. The forward (E12f) and reverse (E17r) primers were targeted to the exon 12 and exon 17, respectively (Weise et al., 2010). The amplicons were TA-cloned and sequenced. All three major isoforms (E, S, M) were found present in the spinal cord.

B, Western blot assay of TCF7l2 in the spinal cord. Both ~79 kD (E isoform) and ~58 kD (M/S isoforms, similar molecular weight) bands were present in the mouse spinal cord and substantially downregulated in P10 TCF7l2 cKO spinal cord (*Olig2-CreER*^{T2}:*Tcf7l2*$^{fl/fl}$, tamoxifen injection at P9). TCF7l2 (clone C48H11, Cell Signaling #2569) was used. GAPDH serves as a loading control.

C, Western blot showing vector-mediated expression of the representative mouse TCF7l2 isoforms (E2, M1, and S2) in the mouse oligodendroglial cell line Oli-Neu cells. Vectors were obtained from (Weise et al., 2010). EV, empty vector.

Figure 2-2: Primary OPC/OL culture and treatment (related to Fig. 2)

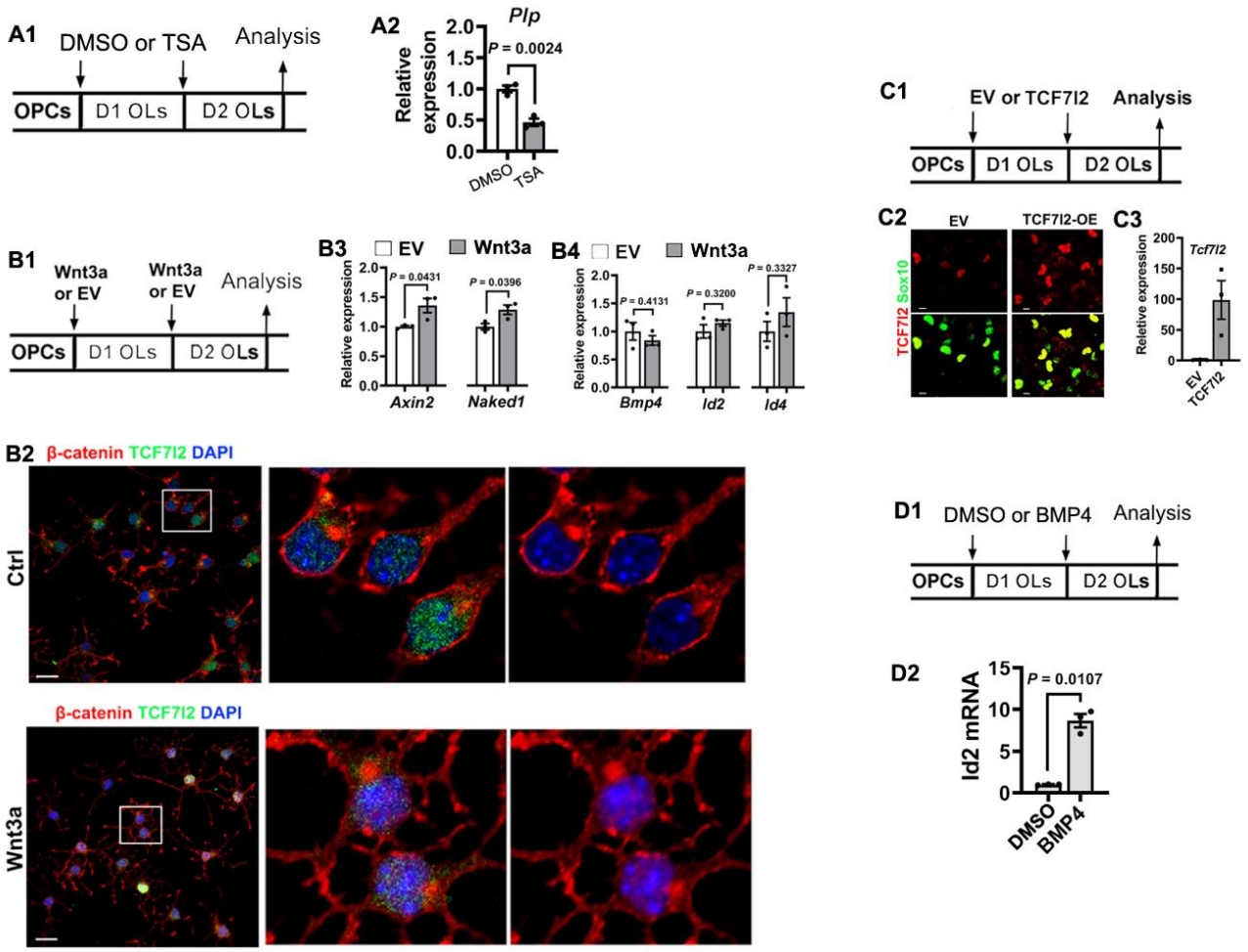

A1, Primary OPCs were purified from neonatal mouse brain. TSA (10ng/ml) or DMSO control was included in the differentiation medium for 48 hours (medium change at 24 hr) prior to analysis. The dose was chosen based on previous study (Marin-Husstege et al., 2002).

A2, RT-qPCR quantification of OL marker *Plp*. Two-tailed *t* test, *t(4)* = 6.830 *Plp*

B1, Mouse primary OPCs was transduced with empty control vector (EV) and vector expressing Wnt3a, a canonical Wnt ligand, at the time of differentiation and analyzed 48 hours after transduction.

B2, confocal images of single optical slice showing localization of β-catenin in Wnt3a-transduced and empty vector-transduced OLs. The boxed areas were shown at higher magnification on the right. Scale bar=10μm.

B3-B4, Relative mRNA levels of Wnt/β-catenin signaling targets *Axin2* and *Naked1* (**E**) and *Bmp4* and BMP4 signaling targets *Id2* and *Id4* (**F**). White bars, Ctrl; gray bars: Wnt3a. Two-

tailed Student's *t* test, $t_{(4)} = 2.924$ *Axin2*, $t_{(4)} = 3.010$ *Naked1*, $t_{(4)} = 0.9126$ *Bmp4*, $t_{(4)} = 1.134$ *Id2*, $t_{(4)} = 1.101$ *Id4*.

C1, Primary OLs were transduced with empty vector (EV) or S2 isoform of TCF7l2 plasmid (TCF7l2 overexpression, TCF7l2-OE), and analyzed at 48 hours post-transduction.

C2-C3, representative confocal images of TCF7l2 and Sox10 and RT-qPCR assay of *Tcf7l2* mRNA in EV and TCF7l2-OE groups.

D1, BMP4 (10ng/ml) or DMSO control was included in the differentiation medium for 48 hours (medium change at 24 hr) prior to analysis.

D2, RT-qPCR quantification of canonical BMP4 signaling target Id2. Two-tailed t test, Welch's corrected $t_{(2.009)} = 9.529$.

Figure 3-1: BMP4 disruption does not affect OL differentiation in vivo (related to Fig. 3)

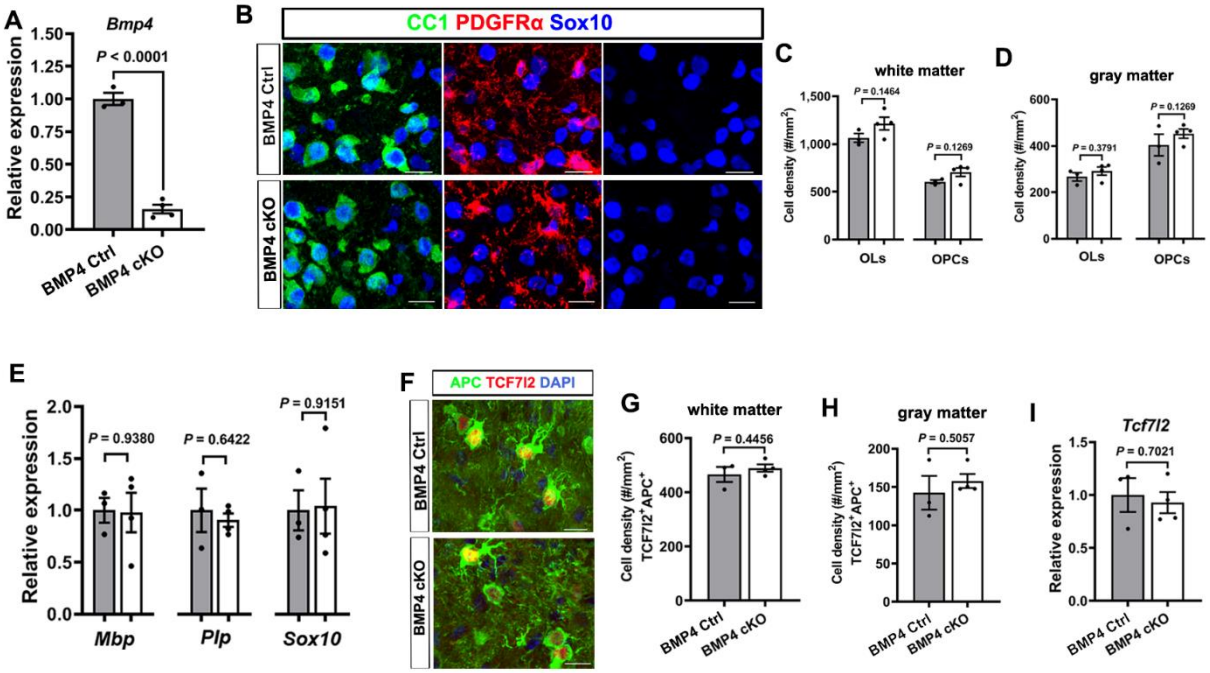

Pdgfrα-CreER^{T2}, *Bmp4*$^{fl/fl}$ (BMP4 cKO) and BMP4 Ctrl (*Bmp4*$^{fl/fl}$) mice were treated with tamoxifen at P5 and P6 and the spinal cord was analyzed at P10.

A, relative *Bmp4* expression by RT-qPCR. Two-tailed Student's *t* test, $t_{(5)}$ = 15.29.

B-D, representative images of Sox10/CC1/PDGFRα IHC (**B**) and densities of Sox10$^+$CC1$^+$ OLs and Sox10$^+$PDGFRα$^+$ OPCs in the spinal white (**C**) and gray (**D**) matter. Scale bar=10μm. Two-tailed *t* test. **C**, $t_{(5)}$ = 1.718 OLs, $t_{(5)}$ = 1.829 OPCs; **D**, $t_{(5)}$ = 0.9646 OLs, $t_{(5)}$ = 1.088 OPCs.

E, relative expression of myelin protein gene *Mbp* and *Plp* and pan-oligodendroglial marker *Sox10* quantified by RT-qPCR. Two-tailed *t* test, $t_{(5)}$ = 0.0817 *Mbp*, $t_{(5)}$ = 0.4940 *Plp,* and $t_{(5)}$ = 0.2660 *Sox10.*

F-H, representative confocal image of newly differentiated OLs labeled by APC/TCF7l2 (**F**), and quantification of APC$^+$/TCF7l2$^+$ cells in the white (**G**) and gray (**H**) matter. Scale bar=10μm. Two-tailed Student's t test, $t_{(5)}$ = 0.8275 white matter, $t_{(5)}$ = 0.7165 gray matter.

I relative Tcf7l2 expression in the spinal cord by RT-qPCR. Two-tailed Student's t test, $t_{(5)}$ = 0.4053.

Table 1 - Detailed information of statistical analyses

Fig.	Sample size (n)	Statistical Methods, t(df) value, F values
1F	n = 4 TCF7l2 Ctrl n = 3 TCF7l2 cKO	Unpaired, two-tailed Student's t test, t(5) = 5.582
1J	n = 4 TCF7l2 Ctrl n = 3 TCF7l2 cKO	Unpaired, two-tailed Student's t test, Welch-corrected t(2.032) = 7.729 Id1, t(5) = 2.910 Id2, t(5) = 3.744 Id3
1K	n = 4 TCF7l2 Ctrl n = 3 Plp-CreERT2:TCF7l2 cKO	Unpaired, two-tailed Student's t test, Welch-corrected t(5.576) = 7.833 Tcf7l2, t(10) = 11.08 Bmp4, t(10) = 3.513 Id3.
2B	n=3 IgG, n = 3 TCF7l2	Unpaired, two-tailed Student's t test, t(4) = 14.00
2C	n = 3 each condition	One-way ANOVA, followed by Tukey's post-test F(2,6) = 11.69, P = 0.0085; * P < 0.05, ** P < 0.01,
2D	n = 3 each condition	One-way ANOVA, followed by Tukey's post-test P = 0.0058; * P < 0.05, ** P < 0.01,
2I	n = 3 DMSO, n = 3 TSA	Unpaired, two-tailed Student's t test, t(4) = 3.328 Bmp4, t(4) = 4.585 Id2
2J	n = 3 EV, n = 3 TCF7l2	Unpaired, two-tailed Student's t test, t(4) = 4.174
2K	n = 3 EV, n = 3 TCF7l2	Unpaired, two-tailed Student's t test, t(4) = 2.960 Mbp, t(4) = 4.458 Plp, t(4) = 3.464 Mog, t(4) = 4.303 Enpp6, and t(4) = 4.976 Myrf
2L	n = 3 EV, n = 3 TCF7l2	Unpaired, two-tailed Student's t test, t(4) = 4.631
2M	n = 3 EV, n = 3 TCF7l2	Unpaired, two-tailed Student's t test, t(4) = 2.839.
2N	n = 3 EV, n = 3 TCF7l2	Unpaired, two-tailed Student's t test, t(4) = 4.976
2O	n = 3 EV, n = 3 TCF7l2	Unpaired, two-tailed Student's t test, t(4) = 0.1368 Axin2, t(4) = 1.724 Nkd1, and t(4) = 1.622 Sp5.
2P	n = 3 each condition	One-way ANOVA, followed by Tukey's post test. F(3, 8) = 25.82, P = 0.0002. ** < 0.01, *** P < 0.001
3B	n = 13 Control n = 4 TCF7l2 cKO n = 4 TCF7l2/BMP4 cKO	One-way ANOVA, followed by Tukey's post-test, F(2,18) = 47.01 P < 0.0001; *** P < 0.001, ns, not significant
3C	n = 13 Control n = 4 TCF7l2 cKO n = 4 TCF7l2/BMP4 cKO	One-way ANOVA, followed by Tukey's post-test, F(2,18) = 87.15 P < 0.0001; *** P < 0.001
3E	n = 3 Control n = 4 TCF7l2 cKO n = 4 TCF7l2/BMP4 cKO	One-way ANOVA, followed by Tukey's post-test, F(2,6) = 10.27, P = 0.0116; * P < 0.05
3G	n = 6 Control n = 3 TCF7l2 cKO n = 4 TCF7l2/BMP4 cKO	One-way ANOVA, followed by Tukey's post-test, F(2,10) = 10.11, P = 0.0040; ** P < 0.01
3H	n = 11 Control n = 4 TCF7l2 cKO n = 4 TCF7l2/BMP4 cKO	One-way ANOVA, followed by Tukey's post-test, F(2,16) = 38.82, P < 0.0001; * P < 0.05, *** P < 0.001

3J	n = 3 Control n = 3 TCF7l2 cKO n = 3 TCF7l2/BMP4 cKO	One-way ANOVA, followed by Tukey's post-test, F(2,6) = 21.30, P = 0.0019; * P < 0.05, ** P < 0.01
3K	n = 3 Control n = 3 TCF7l2 cKO n = 3 TCF7l2/BMP4 cKO	One-way ANOVA, followed by Tukey's post-test, F(2,6) = 13.55, P = 0.0060; * P < 0.05, ** P < 0.01
3M	n = 5 Control n = 4 TCF7l2 cKO n = 5 TCF7l2/BMP4 cKO	One-way ANOVA, followed by Tukey's post-test, F(2,11) = 107.9 P < 0.0001 Sox10+, F(2,11) = 99.72 P < 0.0001 OLs, F(2,11) = 2.945 P = 0.0946 OPCs; ** P < 0.01, **** P < 0.0001, ns, not significant
3N	n = 5 Control n = 4 TCF7l2 cKO n = 5 TCF7l2/BMP4 cKO	One-way ANOVA, followed by Tukey's post-test, F(2,11) = 23.70 P = 0.0001 Sox10+, F(2,11) = 29.91 P < 0.0001 OLs, F(2,11) = 0.4095 P = 0.6737 OPCs; *** P < 0.001, ns, not significant

References:

Angus-Hill, M.L., Elbert, K.M., Hidalgo, J., and Capecchi, M.R. (2011). T-cell factor 4 functions as a tumor suppressor whose disruption modulates colon cell proliferation and tumorigenesis. Proc Natl Acad Sci U S A *108*, 4914-4919.

Armstrong, R.C., Dorn, H.H., Kufta, C.V., Friedman, E., and Dubois-Dalcq, M.E. (1992). Pre-oligodendrocytes from adult human CNS. J Neurosci *12*, 1538-1547.

Boj, S.F., van Es, J.H., Huch, M., Li, V.S., Jose, A., Hatzis, P., Mokry, M., Haegebarth, A., van den Born, M., Chambon, P.*, et al.* (2012). Diabetes risk gene and Wnt effector Tcf7l2/TCF4 controls hepatic response to perinatal and adult metabolic demand. Cell *151*, 1595-1607.

Brazil, D.P., Church, R.H., Surae, S., Godson, C., and Martin, F. (2015). BMP signalling: agony and antagony in the family. Trends Cell Biol *25*, 249-264.

Cadigan, K.M. (2012). TCFs and Wnt/beta-catenin signaling: more than one way to throw the switch. Current topics in developmental biology *98*, 1-34.

Chen, X., Ayala, I., Shannon, C., Fourcaudot, M., Acharya, N.K., Jenkinson, C.P., Heikkinen, S., and Norton, L. (2018). The Diabetes Gene and Wnt Pathway Effector TCF7L2 Regulates Adipocyte Development and Function. Diabetes *67*, 554-568.

Clevers, H. (2006). Wnt/beta-catenin signaling in development and disease. Cell *127*, 469-480.

Costa, C., Eixarch, H., Martinez-Saez, E., Calvo-Barreiro, L., Calucho, M., Castro, Z., Ortega-Aznar, A., Ramon, Y.C.S., Montalban, X., and Espejo, C. (2019). Expression of Bone Morphogenetic Proteins in Multiple Sclerosis Lesions. Am J Pathol *189*, 665-676.

Fancy, S.P., Baranzini, S.E., Zhao, C., Yuk, D.I., Irvine, K.A., Kaing, S., Sanai, N., Franklin, R.J., and Rowitch, D.H. (2009). Dysregulation of the Wnt pathway inhibits timely myelination and remyelination in the mammalian CNS. Genes Dev *23*, 1571-1585.

Franklin, R.J., and Gallo, V. (2014). The translational biology of remyelination: Past, present, and future. Glia.

Gomes, W.A., Mehler, M.F., and Kessler, J.A. (2003). Transgenic overexpression of BMP4 increases astroglial and decreases oligodendroglial lineage commitment. Dev Biol *255*, 164-177.

737 Grinspan, J.B. (2015). Bone Morphogenetic Proteins: Inhibitors of Myelination in Development and
738 Disease. Vitam Horm *99*, 195-222.
739 Grinspan, J.B. (2020). Inhibitors of Myelination and Remyelination, Bone Morphogenetic Proteins, are
740 Upregulated in Human Neurological Disease. Neurochem Res *45*, 656-662.
741 Guo, F., Lang, J., Sohn, J., Hammond, E., Chang, M., and Pleasure, D. (2015). Canonical Wnt signaling in
742 the oligodendroglial lineage-puzzles remain. Glia.
743 Guo, F., Maeda, Y., Ko, E.M., Delgado, M., Horiuchi, M., Soulika, A., Miers, L., Burns, T., Itoh, T., Shen, H.*,*
744 *et al.* (2012). Disruption of NMDA receptors in oligodendroglial lineage cells does not alter their
745 susceptibility to experimental autoimmune encephalomyelitis or their normal development. J Neurosci
746 *32*, 639-645.
747 Hammond, E., Lang, J., Maeda, Y., Pleasure, D., Angus-Hill, M., Xu, J., Horiuchi, M., Deng, W., and Guo, F.
748 (2015). The Wnt effector transcription factor 7-like 2 positively regulates oligodendrocyte differentiation
749 in a manner independent of Wnt/beta-catenin signaling. J Neurosci *35*, 5007-5022.
750 Harlow, D.E., Honce, J.M., and Miravalle, A.A. (2015). Remyelination Therapy in Multiple Sclerosis. Front
751 Neurol *6*, 257.
752 Harnisch, K., Teuber-Hanselmann, S., Macha, N., Mairinger, F., Fritsche, L., Soub, D., Meinl, E., and
753 Junker, A. (2019). Myelination in Multiple Sclerosis Lesions Is Associated with Regulation of Bone
754 Morphogenetic Protein 4 and Its Antagonist Noggin. Int J Mol Sci *20*.
755 Hatzis, P., van der Flier, L.G., van Driel, M.A., Guryev, V., Nielsen, F., Denissov, S., Nijman, I.J., Koster, J.,
756 Santo, E.E., Welboren, W.*, et al.* (2008). Genome-wide pattern of TCF7L2/TCF4 chromatin occupancy in
757 colorectal cancer cells. Mol Cell Biol *28*, 2732-2744.
758 He, Y., Dupree, J., Wang, J., Sandoval, J., Li, J., Liu, H., Shi, Y., Nave, K.A., and Casaccia-Bonnefil, P. (2007).
759 The transcription factor Yin Yang 1 is essential for oligodendrocyte progenitor differentiation. Neuron *55*,
760 217-230.
761 Hull, V., Wang, Y., Burns, T., Zhang, S., Sternbach, S., McDonough, J., Guo, F., and Pleasure, D. (2020).
762 Antisense Oligonucleotide Reverses Leukodystrophy in Canavan Disease Mice. Ann Neurol *87*, 480-485.
763 Hurlstone, A., and Clevers, H. (2002). T-cell factors: turn-ons and turn-offs. The EMBO journal *21*, 2303-
764 2311.
765 Lang, J., Maeda, Y., Bannerman, P., Xu, J., Horiuchi, M., Pleasure, D., and Guo, F. (2013). Adenomatous
766 polyposis coli regulates oligodendroglial development. The Journal of neuroscience : the official journal
767 of the Society for Neuroscience *33*, 3113-3130.
768 Marin-Husstege, M., Muggironi, M., Liu, A., and Casaccia-Bonnefil, P. (2002). Histone deacetylase activity
769 is necessary for oligodendrocyte lineage progression. J Neurosci *22*, 10333-10345.
770 Retting, K.N., Song, B., Yoon, B.S., and Lyons, K.M. (2009). BMP canonical Smad signaling through Smad1
771 and Smad5 is required for endochondral bone formation. Development *136*, 1093-1104.
772 See, J., Mamontov, P., Ahn, K., Wine-Lee, L., Crenshaw, E.B., 3rd, and Grinspan, J.B. (2007). BMP
773 signaling mutant mice exhibit glial cell maturation defects. Molecular and cellular neurosciences *35*, 171-
774 182.
775 Takebayashi, H., Nabeshima, Y., Yoshida, S., Chisaka, O., and Ikenaka, K. (2002). The basic helix-loop-
776 helix factor olig2 is essential for the development of motoneuron and oligodendrocyte lineages. Current
777 biology : CB *12*, 1157-1163.
778 Thompson, D.L., Gerlach-Bank, L.M., Barald, K.F., and Koenig, R.J. (2003). Retinoic acid repression of
779 bone morphogenetic protein 4 in inner ear development. Mol Cell Biol *23*, 2277-2286.
780 Wang, R.N., Green, J., Wang, Z., Deng, Y., Qiao, M., Peabody, M., Zhang, Q., Ye, J., Yan, Z., Denduluri, S.*,*
781 *et al.* (2014). Bone Morphogenetic Protein (BMP) signaling in development and human diseases. Genes
782 Dis *1*, 87-105.

783 Wang, Y., Liu, Q., Xu, Y., Zhang, Y., Lv, Y., Tan, Y., Jiang, N., Cao, G., Ma, X., Wang, J*., et al.* (2016).
784 Ginsenoside Rg1 Protects against Oxidative Stress-induced Neuronal Apoptosis through Myosin IIA-actin
785 Related Cytoskeletal Reorganization. Int J Biol Sci *12*, 1341-1356.
786 Wang, Y., Xu, Y., Liu, Q., Zhang, Y., Gao, Z., Yin, M., Jiang, N., Cao, G., Yu, B., Cao, Z*., et al.* (2017). Myosin
787 IIA-related Actomyosin Contractility Mediates Oxidative Stress-induced Neuronal Apoptosis. Front Mol
788 Neurosci *10*, 75.
789 Weise, A., Bruser, K., Elfert, S., Wallmen, B., Wittel, Y., Wohrle, S., and Hecht, A. (2010). Alternative
790 splicing of Tcf7l2 transcripts generates protein variants with differential promoter-binding and
791 transcriptional activation properties at Wnt/beta-catenin targets. Nucleic Acids Res *38*, 1964-1981.
792 Wenzel, J., Rose, K., Haghighi, E.B., Lamprecht, C., Rauen, G., Freihen, V., Kesselring, R., Boerries, M., and
793 Hecht, A. (2020). Loss of the nuclear Wnt pathway effector TCF7L2 promotes migration and invasion of
794 human colorectal cancer cells. Oncogene *39*, 3893-3909.
795 Wu, M., Hernandez, M., Shen, S., Sabo, J.K., Kelkar, D., Wang, J., O'Leary, R., Phillips, G.R., Cate, H.S., and
796 Casaccia, P. (2012). Differential modulation of the oligodendrocyte transcriptome by sonic hedgehog
797 and bone morphogenetic protein 4 via opposing effects on histone acetylation. J Neurosci *32*, 6651-6664.
798 Ye, B., Li, L., Xu, H., Chen, Y., and Li, F. (2019). Opposing roles of TCF7/LEF1 and TCF7L2 in cyclin D2 and
799 Bmp4 expression and cardiomyocyte cell cycle control during late heart development. Lab Invest *99*,
800 807-818.
801 Ye, F., Chen, Y., Hoang, T., Montgomery, R.L., Zhao, X.H., Bu, H., Hu, T., Taketo, M.M., van Es, J.H.,
802 Clevers, H*., et al.* (2009). HDAC1 and HDAC2 regulate oligodendrocyte differentiation by disrupting the
803 beta-catenin-TCF interaction. Nat Neurosci *12*, 829-838.
804 Zhang, S., Kim, B., Zhu, X., Gui, X., Wang, Y., Lan, Z., Prabhu, P., Fond, K., Wang, A., and Guo, F. (2020).
805 Glial type specific regulation of CNS angiogenesis by HIFalpha-activated different signaling pathways.
806 Nat Commun *11*, 2027.
807 Zhang, S., Rasai, A., Wang, Y., Xu, J., Bannerman, P., Erol, D., Tsegaye, D., Wang, A., Soulika, A., Zhan, X*.,*
808 *et al.* (2018a). The Stem Cell Factor Sox2 Is a Positive Timer of Oligodendrocyte Development in the
809 Postnatal Murine Spinal Cord. Mol Neurobiol.
810 Zhang, S., Zhu, X., Gui, X., Croteau, C., Song, L., Xu, J., Wang, A., Bannerman, P., and Guo, F. (2018b).
811 Sox2 is essential for oligodendroglial proliferation and differentiation during postnatal brain myelination
812 and CNS remyelination. J Neurosci.
813 Zhao, C., Deng, Y., Liu, L., Yu, K., Zhang, L., Wang, H., He, X., Wang, J., Lu, C., Wu, L.N*., et al.* (2016). Dual
814 regulatory switch through interactions of Tcf7l2/Tcf4 with stage-specific partners propels
815 oligodendroglial maturation. Nat Commun *7*, 10883.

816